Meteorol. Z. (Contrib. Atm. Sci.), Vol. **28**, No. 1, 59–67 (published online November 23, 2018)

Characterization of Spread in a Mesoscale Ensemble Prediction System: Multiphysics versus Initial Conditions

Sergio Fernández-González[1], Mariano Sastre[2*], Francisco Valero[2], Andrés Merino[3], Eduardo García-Ortega[3], José Luis Sánchez[3], Jesús Lorenzana[4] and María Luisa Martín[5]

[1]State Meteorological Agency (AEMET), Madrid, Spain
[2]Department of Earth Physics and Astrophysics, Faculty of Physics, Complutense University of Madrid, Madrid, Spain
[3]Atmospheric Physics Group, IMA, University of León, León, Spain
[4]SCAYLE Supercomputación Castilla y León, Spain
[5]Department of Applied Mathematics, Faculty of Computer Engineering, University of Valladolid, Segovia, Spain

(Manuscript received April 5, 2018; in revised form September 5, 2018; accepted October 12, 2018)

Abstract

In this research, uncertainty associated with initial and boundary conditions is evaluated for short-term wind speed prediction in complex terrain. The study area is the Alaiz mountain range, a windy region in the northern Iberian Peninsula. A multiphysics and multiple initial and boundary condition ensemble prediction system (EPS) was generated using the Weather Research and Forecasting model. Uncertainty of the EPS is analyzed using an index based on the spread between ensemble members, considering its behavior under different wind speed and direction events, and also during distinct atmospheric stability conditions. The results corroborate that physical parameterization uncertainty is greater for short-term forecasts (63.5 %). However, it is also necessary to consider the uncertainty associated with initial conditions, not only for its quantitative importance (36.5 %) but also for its behavior during thermal inversion conditions in the narrow valleys surrounded by mountains.

Keywords: wind, physical parameterizations, initial conditions, uncertainty

1 Introduction

In the framework of climate change, the demand for renewable energy is increasing as an alternative to traditional energy sources, which are responsible for the emission of greenhouse gases (Torralba et al., 2017). During recent decades, wind energy has become one of the most economical options for new energy production facilities, and is second in terms of installed capacity (Santos et al., 2015). However, wind energy production needs accurate wind forecasts for integration in the electric grid system (Najafi et al., 2016). In particular, it is vital to accurately estimate the vertical wind profile around the hub height of wind turbines (Draxl et al., 2014). In addition, wind shear and strong gusts may cause structural damage to wind turbines (Worsnop et al., 2017), so the forecast is crucial during extreme wind episodes in order to minimize damage, and for the optimal design of wind farms.

Wind power production prediction is especially important on short time scales, because wind energy producers need to know the power output they will be able to sell in the spot market (Costa et al., 2008). Because global atmospheric models commonly underestimate wind speed (Jiang et al., 2017), the use of mesoscale models is widespread within the scientific community for predicting wind speed at the hub height of wind turbines, especially over complex terrain (Kunz et al., 2010; Graff et al., 2014). In this regard, the Weather Research and Forecasting (WRF) model has been used during recent years for simulating wind flow over complex terrain, with satisfactory results (Hari Prasad et al., 2017). Nevertheless, there is uncertainty in the wind speed forecast even using high-resolution mesoscale models. One solution for estimating this uncertainty is to develop an ensemble composed of several individual simulations (Slingo and Palmer, 2011). The main sources of uncertainty in atmospheric models are related to initial conditions and model errors (Lee et al., 2012). Initial condition uncertainty can be evaluated using data from different global models (Buizza et al., 2005) or by perturbing initial conditions, e.g., with the method known as singular vectors (Molteni and Palmer, 1993). Regarding model errors, uncertainty can be estimated using different models or physics parameterizations, or by modifying parameters in the physics package (Berner et al., 2011). According to Olsen et al. (2017), uncertainty associated with wind speed forecasts by mesoscale models near the ground is mainly associated with physical parameterizations, lead time and spin-up of the model, and grid spacing.

*Corresponding author: Mariano Sastre, Department of Earth Physics and Astrophysics, Faculty of Physics, Complutense University of Madrid. Plaza Ciencias, 1, 28040 Madrid, Spain, e-mail: msastrem@ucm.es

DOI 10.1127/metz/2018/0918
Gebrüder Borntraeger Science Publishers, Stuttgart, www.borntraeger-cramer.com

Table 1: Description of physics parameterizations, initial and boundary conditions used in 16 different simulations.

Simulation code	Boundary conditions	Radiation (shortwave/longwave)	Land surface model	PBL scheme	Surface layer
GFS 121	GFS 0.25°	MM5 / RRTM	NLSM	YSU	MO
GFS 125	GFS 0.25°	MM5 / RRTM	NLSM	MYNN	MYNN
GFS 131	GFS 0.25°	MM5 / RRTM	RUC	YSU	MO
GFS 521	GFS 0.25°	NG / NG	NLSM	YSU	MO
GFS 525	GFS 0.25°	NG / NG	NLSM	MYNN	MYNN
GFS 531	GFS 0.25°	NG / NG	RUC	YSU	MO
ERA 121	ERA 0.75°	MM5 / RRTM	NLSM	YSU	MO
ERA 125	ERA 0.75°	MM5 / RRTM	NLSM	MYNN	MYNN
ERA 131	ERA 0.75°	MM5 / RRTM	RUC	YSU	MO
ERA 521	ERA 0.75°	NG / NG	NLSM	YSU	MO
ERA 525	ERA 0.75°	NG / NG	NLSM	MYNN	MYNN
ERA 531	ERA 0.75°	NG / NG	RUC	YSU	MO

However, an ensemble constructed by considering only model errors tends to be under-dispersive (Buizza et al., 2005).

Therefore, in the present research, an ensemble prediction system (EPS) was developed that considers both initial and boundary conditions and model errors. The aim was to minimize the under-dispersive nature of EPSs (Hamill and Colucci, 1997). The WRF mesoscale model was selected because of its versatility, allowing the use of different initial conditions and multiple physical parameterizations to build the ensemble. The main goal was to analyze the influence of both initial and boundary conditions and physical schemes in the generation of spread over the study area, evaluating uncertainty depending on wind speed and direction, atmospheric stability in the planetary boundary layer (PBL), and reasons for the geographic distribution of the spread.

The paper is structured as follows. In Section 2, the materials and methods are explained, including characteristics of the model, the index used for uncertainty estimation, and the study area. Next, the experiments developed and results are presented. Finally, an integrated discussion and conclusions are given.

2 Materials and methods

2.1 WRF model setup

Version 3.6.1 of the WRF model was used for developing the simulations used in this research. It is a non-hydrostatic mesoscale model (Skamarock and Klemp, 2008) that is commonly used within the scientific community. It has been proven a successful tool to simulate atmospheric conditions for studying different meteorological issues, including sea-breeze phenomena (Arrillaga et al., 2016), severe storms (Gascón et al., 2015a), aircraft icing (Fernández–González et al., 2014), radiation fog (Román-Cascón et al., 2016), snowfall events (Fernández-González et al., 2015; Gascón et al., 2015b), and PBL evening transition (Sastre et al., 2012). For the specific case of wind energy, the WRF model has also been used successfully (Argüeso and Businger, 2018). Regarding initial and boundary conditions, the ERA-Interim reanalysis (ERA) and National Centers for Environmental Prediction Global Forecast System (NCEP-GFS) analysis were selected, following the recommendations of Carvalho et al. (2014). As a result, two sets of simulations were defined by using distinct initial and boundary conditions, i.e., NCEP-GFS analysis with 0.25° grid size (Saha et al., 2010) and ERA reanalysis with horizontal resolution 0.75° (Dee et al., 2011). In addition, various land surface model, surface layer, radiation, and PBL parameterizations were used for evaluating model error, giving 16 different simulations. For the parameterization of radiation, the MM5 shortwave scheme (Dudhia, 1989) and Rapid Radiative Transfer Model (RRTM, Mlawer et al., 1997) were tested in one set of simulations, and new Goddard (NG) shortwave and longwave radiation schemes (Chou et al., 2001) were tested in the other. Regarding the PBL scheme, the Yonsei University (YSU) parameterization (Hong et al., 2006) and Mellor-Yamada-Nakanishi-Niino (MYNN) scheme (Nakanishi and Niino, 2006) were used, because these two are often the best performing for local wind and boundary-layer characteristics (Hari-Prasad et al., 2017). The Noah Land Surface Model (NLSM, Chen and Dudhia, 2001) and the Rapid Update Cycle (RUC, Smirnova et al., 1997) were selected for surface processes. In addition, the default land use and land cover datasets included in the GFS 0.25 and ERA-Interim databases are the ones considered. Table 1 shows a summary of all these combinations. More information about the WRF model configuration for these simulations can be found in Fernández-González et al. (2018).

We selected 15 days in May 2015, previously tested and compared with observational wind measurements by Fernández-González et al. (2018). These include episodes with various wind intensities and directions and atmospheric static stability conditions, whose relative frequency can also be consulted in Fernández–González et al. (2018). The simulations were initial-

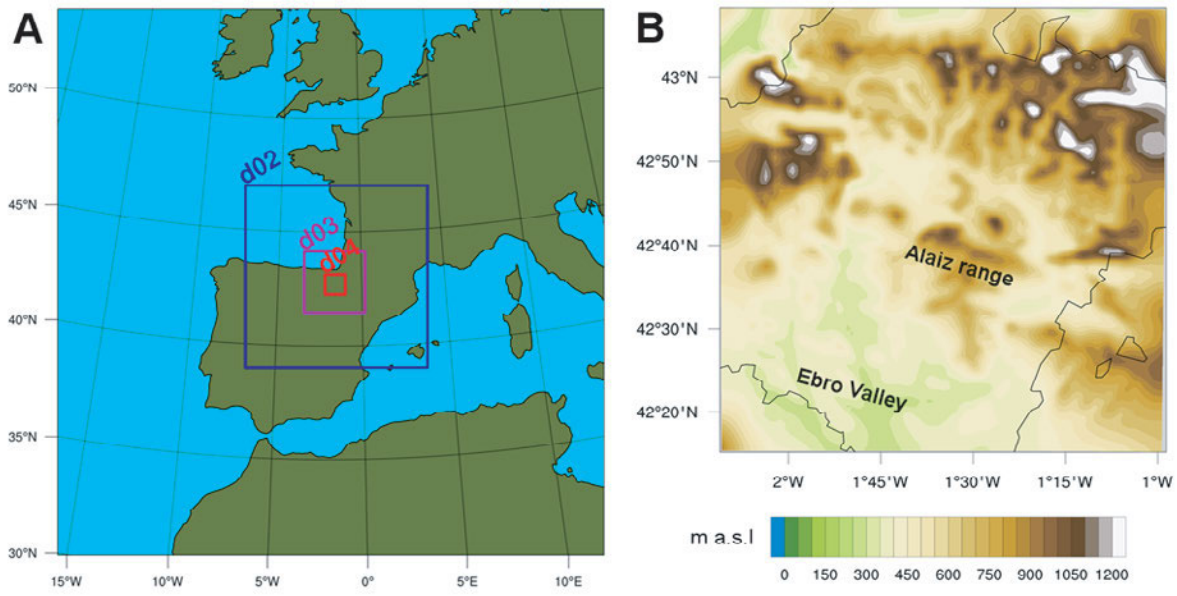

Figure 1: WRF domain configuration (A) and orography of study area (B). Region shown in Fig. 1B coincides with domain 4 indicated in Fig. 1A.

ized at 0000 UTC, with a temporary scope of 36 h and the first 12 h considered a spin-up period. Four nested domains with 100 × 100 grid points each were defined following a two-way nesting strategy, resulting in horizontal resolutions of 27, 9, 3, and 1 km (Fig. 1A). A total of 61 sigma levels were used, with greater resolution in lower levels to better simulate PBL processes.

2.2 Spread index

One of the most frequently used solutions to quantify uncertainty associated with an EPS is to evaluate the existing spread between ensemble members (Grimit and Mass, 2007). During recent decades, several spread indexes have been defined using different methods (Hopson, 2014). In particular, various spread indexes defined in Fernández-González et al. (2017) were considered for use in our research, taking into account the peculiarities of the EPS examined.

In the sensitivity analysis of Fernández-González et al. (2018) for the same EPS, four ensemble members were highlighted for results markedly worse than the others. Those members used both the RUC land surface model and MYNN PBL parameterization in the same simulation. In order not to include potential outliers derived from inadequate interactions between these parameterizations, the aforesaid four ensemble members were disregarded in estimation of the spread index (SI), and the results obtained by these four simulations were not used at all in this work. With the aim of not increasing the slightly under-dispersive nature of the EPS, as detected by Fernández-González et al. (2018) when comparing the simulations with wind measurements in the study area, all remaining ensemble members were used for that estimation, resulting in an EPS composed of 12 ensemble members (EPS12). As a result, a modification of the SI defined by Fernández-González et al. (2017) was used:

$$SI = \left(\frac{EPS12maximum - EPS12minimum}{EPS12mean} \right) \times 100 \tag{2.1}$$

It should be noted that the variable used in this work to calculate the SI index is the wind speed at 90 m above ground level (a.g.l.) to be representative of the wind at the hub height of wind turbines.

2.3 Study area

We selected a region in the northern Iberian Peninsula, the Alaiz mountain range, where several wind farms are located (Fig. 1B). The study area is at the confluence of two of the windiest regions of the peninsula, the Upper Ebro Valley and the Eastern Cantabrian (Lorente–Plazas et al., 2015). This region is characterized by complex terrain, making necessary the use of mesoscale models for proper simulation of wind flow. A complete description of the study area is in Sanz Rodrigo et al. (2013).

3 Results

3.1 Wind speed analysis

First, we describe wind speeds across the study area during the 15 selected days, which is very helpful for the analysis of spread spatial resolution analyzed in the following subsections. Fig. 2 shows the temporal average (A) and variance (B) of wind speed at 90 m a.g.l. in domain 4, obtained by the ensemble mean of the WRF

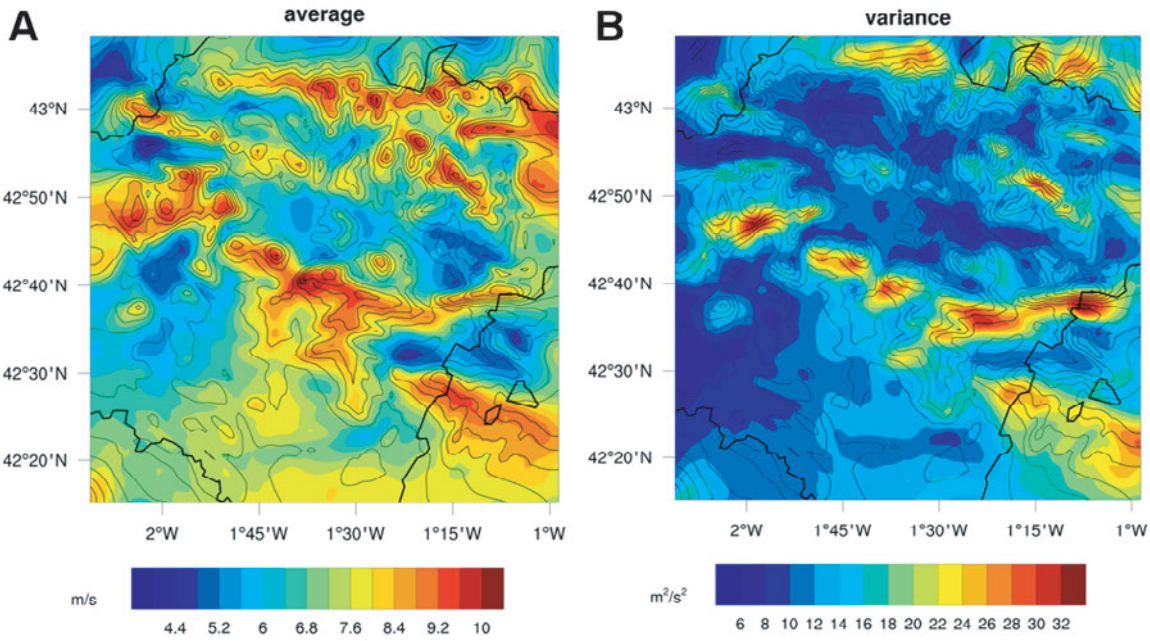

Figure 2: Temporal average (A) and variance (B) of wind speed at 90 m a.g.l. in domain 4, simulated by WRF ensemble mean during study period.

model during the study period. In Fig. 2A, the strongest winds are at the highest elevations, coinciding with the mountain ranges. On the contrary, weaker wind speeds are evident in the small valleys, but not the Ebro Valley (Figs. 2 and 1B). In that valley, the wind is usually channeled, so it attains large values.

Subsequently, over the 15 days of the study period, variance of the wind speed ensemble mean was estimated at each grid point of domain 4 (Fig. 2B). In that way, temporal variance of the simulated wind speed during the study period was obtained. It is remarkable that greater variance is seen on the leeward side of orographic barriers, considering that northerly winds prevail in the study area, as demonstrated by observational measurements analyzed in Fernández–González et al. (2018). In the rest of domain 4, the variance is less, indicating a more stable wind speed.

3.2 Uncertainty quantification: vertical and temporal evolution of spread

In this subsection, the uncertainty is evaluated by means of the SI. In this endeavor, the uncertainty quantification was analyzed under different scenarios. First, the episodes were distinguished as a function of wind speed. When the ensemble mean speed at 90 m a.g.l. was $> 7\,\mathrm{m\,s^{-1}}$ (considered a reference value because it was approximately the average wind speed in domain 4 during the study period), the event was categorized as one of "strong wind". A wind speed $< 7\,\mathrm{m\,s^{-1}}$ was defined as a "weak wind" event. Second, regarding the wind direction at 90 m a.g.l from the ensemble mean, we differentiated between north wind (wind direction 0° ± 60°) and south wind (180° ± 60°) events. Finally, the events were separated depending on atmospheric static stability, which was estimated by potential temperature (θ) at 38 and 97 m a.g.l. (for being consistent with the methodology followed by Fernández-González et al., 2018), estimated by the ensemble mean. As a result, the events were categorized as "unstable" ($\mathrm{d}\theta/\mathrm{d}z < 0$), "neutral" ($\mathrm{d}\theta/\mathrm{d}z = 0$), "stable" ($\mathrm{d}\theta/\mathrm{d}z > 0$), and "thermal inversion".

Fig. 3A shows SI average values at different heights in domain 4 throughout the study period, under distinct meteorological situations. It is remarkable that the spread, and consequently the uncertainty, during weak wind episodes (95 %–97 %) was almost double that of strong wind episodes (45 %–52 %). Because the SI values are percentages, this difference cannot be attributed to the magnitude difference between weak and strong wind events. In the same way, uncertainty was considerably greater during southern wind events (79 %–82 %) than northern ones (60 %–63 %). Indeed, after analyzing the database, we found that strong wind events were related to northerly winds, and weak wind events mainly connected to southerly winds. Therefore, episodes of strong winds with a northerly component are very predictable in the study area. On the contrary, forecast uncertainty increases markedly during episodes of weak winds with a southerly component. The reason may be that the orography is much more complex south of the study area, which creates strong turbulence with southerly winds (Sanz Rodrigo et al., 2013). The flow is much less turbulent under winds with a northerly component, because the wind comes from the Cantabrian Sea and is channeled by the orography to the study area (Lorente-Plazas et al., 2015).

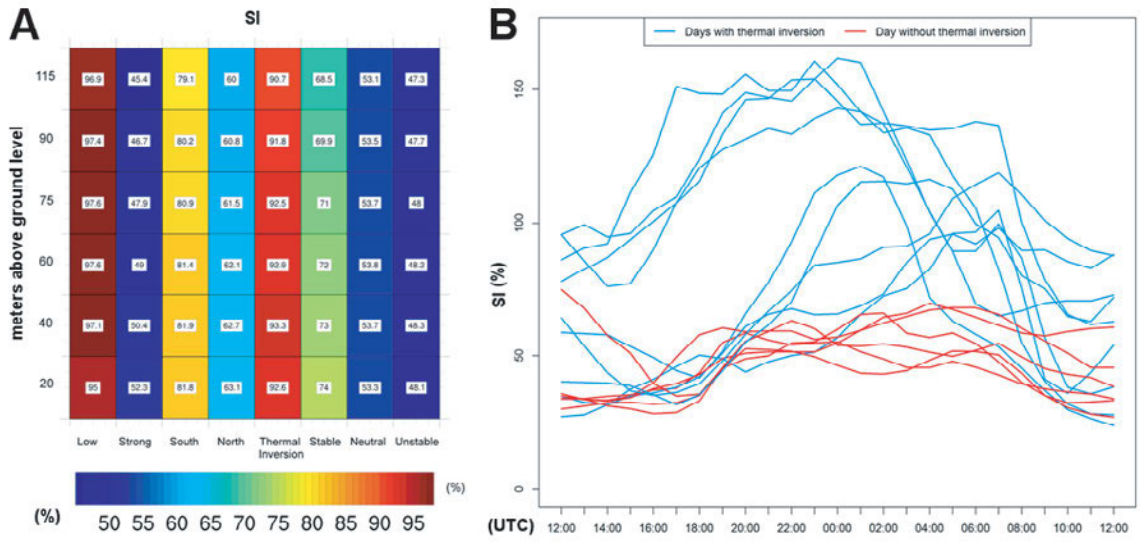

Figure 3: Average SI during study period in domain 4 at different heights under distinct meteorological conditions (A). Daily evolution of SI at 90 m a.g.l. during days with (blue) and without (red) thermal inversion (B).

Among the results according to static atmospheric stability, a remarkable decline of uncertainty was observed for more unstable static stability. Therefore, the greatest uncertainty was during thermal inversion situations (SI = 90 %–93 %). The spread was still large when the static atmospheric stability was categorized as stable (68 %–74 %), but the forecast was more predictable during neutral (53 %–54 %) and unstable (47 %–48 %) conditions. These results are consistent with those of Fernández-González et al. (2018), who claimed that wind speed is less predictable during thermal inversions.

Concerning the uncertainty at different heights, it increased (larger SI values) at lower levels of the PBL (except during weak wind events). This effect was more noticeable during strong wind events, and when the PBL was stable. The greater uncertainty at the lower levels of the PBL might be caused by errors associated with the physical parameterizations (Frediani et al., 2016).

Subsequently, we investigated the temporal evolution of the spread. The behavior was very different during days characterized by thermal inversions during nighttime, so we decided to differentiate it in Fig. 3B. During episodes without a thermal inversion (red lines in Fig. 3B), a daily cycle is not evident in the SI values, because the uncertainty does not show great differences between day and night. However, events characterized by a thermal inversion show a daily cycle in which the uncertainty is much greater during the nighttime (coinciding with the development of a thermal inversion layer in the PBL), with a more predictable wind flow during the diurnal period. Fernández-González et al. (2018) observed a diurnal cycle of wind speed when the PBL was statically stable in the study area, with stronger wind speeds during daytime, mainly because of radiative processes. The reason may be that stability decreases during the daytime, while wind speed increases. This reduces the uncertainty because, as mentioned above, strong wind and unstable events are more predictable.

3.3 Spatial distribution of uncertainty

Finally, the spatial distribution of uncertainty within the study area was evaluated. In addition, we examined the uncertainty linked to physical parameterizations (by measuring only the spread within the ensemble members as generated by a specific initial condition database) or initial and boundary conditions for various scenarios of wind speed and direction and of atmospheric static stability.

Fig. 4A–H shows the SI caused only by the physical parameterizations. The spread associated with those parameterizations represents 63.5 % of the total spread, and was thus the main source of uncertainty in the EPS developed herein. During southern wind events (Fig. 4B), there were several strong uncertainty regions, mainly in low-altitude areas. The pattern is similar for weak wind situations (Fig. 4A), although moderate-to-high uncertainty is widespread over the study area (except at higher altitudes). For northern wind episodes (Fig. 4F), the uncertainty is considerably less than in the case of a south wind component (Fig. 4B). However, the appearance of several areas of moderate uncertainty is remarkable, which are on the leeward side of the orographic barriers (Fig. 1B). This pattern is similar in the strong wind panel (Fig. 4E), reaffirming that strong wind episodes are mainly related to the north wind component. In conditional and unstable conditions (Fig. 4G and H), there is an area of moderate uncertainty in the northwest part of the study are, coinciding with a narrow gorge of West–East orientation (Fig. 1B). This orientation can produce a shadow effect during northerly and southerly wind episodes, causing weak winds (as seen in

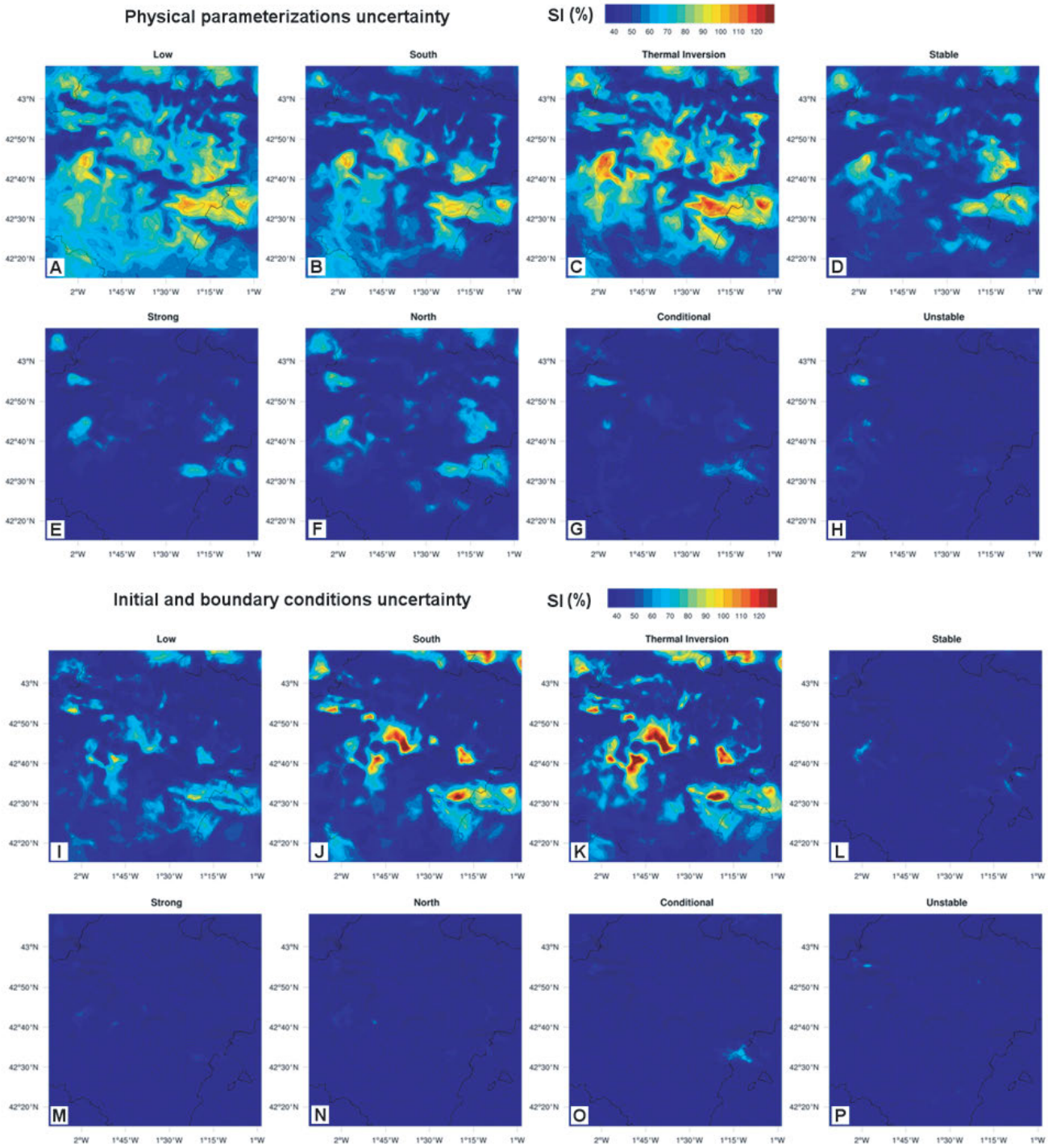

Figure 4: Average SI in domain 4 under distinct meteorological conditions generated only by physical parameterization uncertainties (A–H), and only by initial condition uncertainties (I–P).

Fig. 2A) that are, as mentioned above, less predictable. When the PBL was categorized as stable (Fig. 4D), the configuration shows a strong similarity to the northerly wind events, but with greater uncertainty. Nevertheless, the most impressive results appeared when a thermal inversion layer was present in the PBL (Fig. 4C), with SI values exceeding 100 %. In these cases, the uncertainty was extraordinarily great in the valleys of the study area (Fig. 1B), with the exception of the Ebro Valley, which apparently does not experience this process. The reason may be the wind channelling effect, which makes wind speed more predictable in that valley.

Initial and boundary conditions only contributed 36.5 % of the total spread, although the uncertainty that initial conditions produced cannot be ignored because it is very important during certain weather conditions. As shown in Fig. 4I–P, there are extremely large SI values in the small valleys during thermal inversion and southerly

wind component periods (Fig. 4J and K). It is in these cases when the uncertainty from initial and boundary conditions is critical. During weak wind events (Fig. 4I), the uncertainty pattern is similar to that of southerly wind component episodes, but the SI is smaller. For the remaining scenarios (strong winds, northerly wind components, and stable, conditional, and unstable situations; Fig. 4L–P), uncertainty associated with initial conditions is almost negligible.

Regions with greater variance (Fig. 2B) are not strictly associated with poor predictability (Fig. 4). For example, small valleys, which are characterized by small variance, stand out for having the greatest uncertainty. Therefore, wind speed variance for a specific location and period cannot always be associated with high or low predictability.

4 Discussion and conclusions

In general terms, the uncertainty associated with model errors is prevalent in short-term forecasts, because the spread grows faster in ensembles developed by combining different physical parameterizations rather than those developed by considering only different initial conditions (Stensrud et al., 2000). This is consistent with most of the results in the present work, although our findings indicate that considering both sources of uncertainty is very advantageous under certain weather conditions. In particular, the uncertainty generated by initial and boundary conditions during thermal inversion conditions may be related to distinct inputs of relative humidity, especially at the surface level, a characteristic considered in the initial conditions of the NCEP-GFS analysis and ERA-Interim reanalysis. The importance of nearby moisture at the surface has also been observed during the transition from a diurnal convective to nocturnal stable boundary layer (Sastre et al., 2015). This influences all the other PBL meteorological variables, including wind speed. It is also possible that the higher spatiotemporal resolution of the NCEP-GFS analysis gives more reliable initial conditions over complex terrain under certain weather conditions, such as the formation of a thermal inversion layer in the PBL during nighttime (Fernández-González et al., 2018) and the forecast of land surface skin temperature during daytime (Zheng et al., 2012). Regarding physical parameterizations, the two PBL schemes considered in the EPS herein produced uncertainty, because MYNN PBL scheme estimates of wind speed are frequently smaller than those from the YSU PBL parameterization, sometimes causing underestimation of wind speed (Fernández-González et al., 2018). Results for the radiation schemes are not as unequivocal as the former, and for this reason they require further analysis.

The main conclusions of this study can be summarized as follows:

- Areas with stronger winds stand out for having greater predictability, which is very advantageous for wind energy purposes.
- Greater variance is associated with the leeward side of orographic barriers and in small valleys.
- In the vertical wind profile, uncertainty decreases with height (except during weak wind events and thermal inversion conditions).
- Strong northerly wind episodes show little forecast uncertainty, but uncertainty increases markedly in weak southerly wind events.
- Regarding static atmospheric stability, diminishing uncertainty was observed from stable to unstable static stabilities. The greatest uncertainty was for thermal inversion conditions. This appears to be linked to the observed diurnal cycle of ensemble spread when a thermal inversion layer was developed in the PBL, with greater uncertainty during nighttime.
- Although uncertainty generated by different physical parameterizations is quantitatively greater, the uncertainty caused by initial conditions cannot be discarded because it provides considerable information under certain weather conditions, especially southerly wind and thermal inversion episodes.

In future research, our method will be applied to wider areas to see if the conclusions can be extended to other regions. The results from this research can be useful for the selection of the most viable locations for installing wind farms. Such locations should not only be chosen based on wind strength but also on uncertainty in the wind speed forecast.

Acknowledgments

This work was partially supported by research projects METEORISK (RTC-2014-1872-5), PCIN-2014-013-C07-04 and PCIN2016-080 (UE ERA-NET Plus NEWA Project), ESP2013-47816-C4-4-P, CGL2010-15930, CGL2016-78702-C2-1-R and CGL2016-78702-C2-2-R, CGL2016-81828-REDT, and the Instituto de Matemática Interdisciplinar (IMI) of the Universidad Complutense. Special thanks go to Steven Hunter and Analisa Weston. To request the data, please contact S. Fernández-González (sfernandezg@aemet.es).

References

Argüeso, D., S. Businger, 2018: Wind power characteristics of Oahu, Hawaii. – Renew. Energ. **128**, 324–336, DOI:10.1016/j.renene.2018.05.080.

Arrillaga, J.A., C. Yagüe, M. Sastre, C. Román-Cascón, 2016: A characterisation of sea-breeze events in the eastern Cantabrian coast (Spain) from observational data and WRF simulations. – Atmos. Res. **181**, 265–280, DOI:10.1016/j.atmosres.2016.06.021.

Berner, J., S.-Y. Ha, J.P. Hacker, A. Fournier, C. Snyder, 2011: Model Uncertainty in a Mesoscale Ensemble Prediction System: Stochastic versus Multiphysics Representations. – Mon. Wea. Rev. **139**, 1972–1995, DOI:10.1175/2010MWR3595.1.

Buizza, R., P.L. Houtekamer, Z. Toth, G. Pellerin, M. Wei, Y. Zhu, 2005: A comparison of the ECMWF, MSC, and NCEP Global Ensemble Prediction Systems. – Mon. Wea. Rev. **133**, 1076–1097, DOI:10.1175/MWR2905.1.

Carvalho, D., A. Rocha, M. Gómez-Gesteira, C. Silva Santos, 2014: WRF wind simulation and wind energy production estimates forced by different reanalyses: Comparison with observed data for Portugal. – Appl. Energy, **117**, 116–126, DOI: 10.1016/j.apenergy.2013.12.001.

Chen, F., J. Dudhia, 2001: Coupling and advanced land surface-hydrology model with the Penn State-NCAR MM5 modeling system. Part I: Model implementation and sensitivity. – Mon. Wea. Rev. **129**, 569–585, DOI:10.1175/1520-0493(2001)129<0569:CAALSH>2.0.CO;2.

Chou, M.-D., M.J. Suárez, X. -Z. Liang, M.M.-H. Yan, 2001: A thermal infrared radiation parameterization for atmospheric studies. – Technical Report Series on Global Modeling and Data Assimilation, NASA/TM-2001-104606, Vol. **19**, Goddard Space Flight Center, 56 pp.

Costa, A., A. Crespo, J. Navarro, G. Lizcano, H. Madsen, E. Feitosa, 2008: A review on the young history of the wind power short-term prediction. – Renew. Sustain. Energy Rev. **12**, 1725–1744, DOI:10.1016/j.rser.2007.01.015.

Dee, D.P., S.M. Uppala, A.J. Simmons, P. Berrisford, P. Poli, S. Kobayashi, U. Andrae, M.A. Balmaseda, G. Balsamo, P. Bauer, P. Bechtold, A.C. Beljaars, L. van de Berg, J. Bidlot, N. Bormann, C. Delsol, R. Dragani, M. Fuentes, A.J. Geer, L. Haimberger, S.B. Healy, H. Hersbach, E.V. Hólm, L. Isaksen, P. Kållberg, M. Köhler, M. Matricardi, A.P. McNally, B.M. Monge-Sanz, J. Morcrette, B. Park, C. Peubey, P. de Rosnay, C. Tavolato, J. Thépaut, F. Vitart, 2011: The ERA-interim reanalysis: Configuration and performance of the data assimilation system. – Quart. J. Roy. Meteor. Soc. **137**, 553–597, DOI:10.1002/qj.828.

Draxl, C., A.N. Hahmann, A. Peña, G. Giebel, 2014: Evaluating winds and vertical wind shear from weather research and forecasting model forecasts using seven planetary boundary layer schemes. – Wind Energy, **17**, 39–55, DOI:10.1002/we.1555.

Dudhia, J., 1989: Numerical study of convection observed during the winter monsoon experiment using a mesoscale two-dimensional model. – J. Atmos. Sci. **46**, 3077–107.

Fernández-González, S., J.L. Sánchez, E. Gascón, L. López, E. García-Ortega, A. Merino, 2014: Weather Features Associated with Aircraft Icing Conditions: A Case Study. – The Scientific World Journal, 2014, Article ID 279063, 18 pp, DOI:10.1155/2014/279063.

Fernández-González, S., F. Valero, J.L. Sánchez, E. Gascón, L. López, E. García-Ortega, A. Merino, 2015: Numerical simulations of snowfall events: Sensitivity analysis of physical parameterizations. – J. Geophys. Res. **120**, 10130–10148, DOI:10.1002/2015JD023793.

Fernández-González, S., M.L. Martín, A. Merino, J.L. Sánchez, F. Valero, 2017: Uncertainty uantification and predictability of wind speed over the Iberian Peninsula. – J. Geophys. Res. Atmos. **122**: 3877–3890, DOI:10.1002/2017JD026533.

Fernández-González, S., M.L. Martín, E. García-Ortega, A. Merino, J. Lorenzana, J.L. Sánchez, F. Valero, J. Sanz Rodrigo, 2018: Sensitivity analysis of WRF model: wind-resource assessment for complex terrain. – J. Appl. Meteor. Climatol. **57**, 733–753, DOI:10.1175/JAMC-D-17-0121.1.

Frediani, M.E.B., J.P. Hacker, E.N. Anagnostou, T. Hopson, 2016: Evaluation of PBL Parameterizations for Modeling Surface Wind Speed during Storms in the Northeast United States. – Wea. Forecast. **31**, 1511–1528, DOI: 10.1175/WAF-D-15-0139.1.

Gascón, E., A. Merino, J.L. Sánchez, S. Fernández-González, E. García-Ortega, L. López, L. Hermida, 2015a: Spatial distribution of thermodynamic conditions of severe storms in southwestern Europe. – Atmos. Res. **164–165**, 194–209, DOI:10.1016/j.atmosres.2015.05.012.

Gascón, E., J.L. Sánchez, D. Charalambous, S. Fernández-González, L. López, E. García-Ortega, A. Merino, 2015b: Numerical diagnosis of a heavy snowfall event in the center of the Iberian Peninsula. – Atmos. Res. **153**, 250–263, DOI:10.1016/j.atmosres.2014.08.001.

Graff, M., R. Peña, A. Medina, H.J. Escalante, 2014: Wind speed forecasting using a portfolio of forecasters. – Renew. Energy, **68**, 550–559, DOI:10.1016/j.renene.2014.02.041.

Grimit, E.P., C.F. Mass, 2007: Measuring the ensemble spread–error relationship with a probabilistic approach: Stochastic ensemble results. – Mon. Wea. Rev. **135**, 203–221, DOI:10.1175/MWR3262.1.

Hamill, T.M., S.J. Colucci, 1997: Verification of Eta-RSM short-range ensemble forecasts. – Mon. Wea. Rev. **125**, 1312–1327.

Hari Prasad, K.B.R.R., C.V. Srinivas, T.N. Rao, C.V. Naidu, R. Baskaran, 2017: Performance of WRF in simulating terrain induced flows and atmospheric boundary layer characteristics over the tropical station Gadanki. – Atmos. Res. **185**, 101–17, DOI:10.1016/j.atmosres.2016.10.020.

Hong, S. -Y., Y. Noh, J. Dudhia, 2006: A new vertical diffusion package with an explicit treatment of entrainment processes. – Mon. Wea. Rev. **134**, 2318–2341, DOI:10.1175/MWR3199.1.

Hopson, T.M., 2014: Assessing the ensemble spread–error relationship. – Mon. Wea. Rev. **142**, 1125–1142, DOI: 10.1175/MWR-D-12-00111.1.

Jiang, Y., X. Xu, H. Liu, X. Dong, W. Wang, G. Jia, 2017: The underestimated magnitude and decline trend in near-surface wind over China. – Atmos. Sci. Lett. **18**, 475–483, DOI: 10.1002/asl.791.

Kunz, M., S. Mohr, M. Rauthe, R. Lux, C. Kottmeier, 2010: Assessment of extreme wind speeds from regional climate models – part 1: Estimation of return values and their evaluation. – Nat. Hazards Earth Syst. Sci. **10**, 907–922, DOI: 10.5194/nhess-10-907-2010.

Lee, J.A., W.C. Kolczynski, T.C. Mccandless, S.E. Haupt, 2012: An objective methodology for configuring and down-selecting an NWP ensemble for low-level wind prediction. – Mon. Wea. Rev. **140**, 2270–2286, DOI:10.1175/MWR-D-11-00065.1.

Lorente-Plazas, R., J.P. Montávez, P.A. Jiménez, S. Jerez, J.J. Gómez-Navarro, J.A. García-Valero, P. Jiménez-Guerrero, 2015: Characterization of Surface winds over the Iberian Peninsula. – Int. J. Climatol. **35**, 1007–1026, DOI: 10.1002/joc.4034.

Mlawer, E.J., S.J. Taubman, P.D. Brown, M.J. Iacono, S.A. Clough, 1997: Radiative transfer for inhomogeneous atmospheres: RRTM, a validated correlated-k model for the longwave. – J. Geophys. Res. D. Atmos. **102**, 16663–16682, DOI:10.1029/97JD00237.

Molteni, F., T.N. Palmer, 1993: Predictability and finite-time instability of the northern winter circulation. – Quart. J. Roy. Meteor. Soc. **119**, 269–298, DOI:10.1002/qj.49711951004.

Najafi, A., H. Falaghi, J. Contreras, M. Ramezani, 2016: Medium-term energy hub management subject to electricity price and wind uncertainty. – Appl. Energy, **168**, 418–433, DOI:10.1016/j.apenergy.2016.01.074.

Nakanishi, M., H. Niino, 2006: An improved Mellor-Yamada level-3 model: Its numerical stability and application to a regional prediction of advection fog. – Bound.-Layer Meteor. **119**, 397–407, DOI:10.1007/s10546-005-9030-8.

Olsen, B.T., A.N. Hahmann, A.M. Sempreviva, J. Badger, H.E. Jørgensen, 2017: An intercomparison of mesoscale models at simple sites for wind energy applications. – Wind Energ. Sci. **2**, 211–228, DOI:10.5194/wes-2-211-2017.

Román-Cascón, C., C. Yagüe, G.-J. Steeneveld, M. Sastre, J.A. Arrillaga, G. Maqueda, 2016: Estimating fog-top height through near-surface micrometeorological measurements. – Atmos. Res. **170**, 76–86, DOI:10.1016/j.atmosres.2015.11.016.

Saha, S., S. Moorthi, H.-L. Pan, X. Wu, J. Wang, S. Nadiga, P. Tripp, R. Kistler, J. Woollen, D. Behringer, H. Liu, D. Stokes, R. Grumbine, G. Gayno, J. Wang, Y.-T. Hou, H.-Y. Chuang, H.-M.H. Juang, J. Sela, M. Iredell, R. Treadon, D. Kleist, P.V. Delst, D. Keyser, J. Derber, M. Ek, J. Meng, H. Wei, R. Yang, S. Lord, H.V.D. Dool, A. Kumar, W. Wang, C. Long, M. Chelliah, Y. Xue, B. Huang, J.-K. Schemm, W. Ebisuzaki, R. Lin, P. Xie, M. Chen, S. Zhou, W. Higgins, C.-Z. Zou, Q. Liu, Y. Chen, Y. Han, L. Cucurull, R.W. Reynolds, G. Rutledge, M. Goldberg, 2010: The NCEP climate forecast system reanalysis. – Bull. Amer. Meteor. Soc. **91**, 1015–57, DOI:10.1175/2010BAMS3001.1.

Santos, J., C. Rochinha, M. Liberato, M. Reyers, J. Pinto, 2015: Projected changes in wind energy potentials over Iberia. – Renew. Energy **75**, 68–80, DOI:10.1016/j.renene.2014.09.026.

Sanz Rodrigo, J., F. Borbón Guillén, P. Gómez Arranz, M.S. Courtney, R. Wagner, E. Dupont, 2013: Multi-site testing and evaluation of remote sensing instruments for wind energy applications. – Renew. Energy **53**, 200–210, DOI:10.1016/j.renene.2012.11.020.

Sastre, M., C. Yagüe, C. Román-Cascón, G. Maqueda, F. Salamanca, S. Viana, 2012: Evening transitions of the atmospheric boundary layer: characterization, case studies and WRF simulations. – Adv. Sci. Res. **8**, 39–44, DOI:10.5194/asr-8-39-2012.

Sastre, M., C. Yagüe, C. Román-Cascón, G. Maqueda, 2015: Atmospheric boundary-layer evening transitions: a comparison between two different experimental sites. – Bound.-Layer Meteor. **157**, 375–399, DOI:10.1007/s10546-015-0065-1.

Skamarock, W.C., J.B. Klemp, 2008: A time-split nonhydrostatic atmospheric model for weather research and forecasting applications. – J. Comput. Phys. **227**, 3465–85, DOI:10.1016/j.jcp.2007.01.037.

Slingo, J., T. Palmer, 2011: Uncertainty in weather and climate prediction. – Philos. Trans. Roy. Soc. London, A369, 4751–4767, DOI:10.1098/rsta.2011.0161.

Smirnova, T.G., J.M. Brown, S.G. Benjamin, 1997: Performance of different soil model configurations in simulating ground surface temperature and surface fluxes. – Mon. Wea. Rev. **125**, 1870–1884, DOI:10.1175/1520-0493(1997)125<1870:PODSMC>2.0.CO;2.

Stensrud, D., J.-W. Bao, T. Warner, 2000: Using initial condition and model physics perturbations in short-range ensemble simulations of mesoscale convective systems. – Mon. Wea. Rev. **128**, 2077–2107, DOI:10.1175/1520-0493(2000)128<2077:UICAMP>2.0.CO;2.

Torralba, V., F.J. Doblas-Reyes, D. MacLeod, I. , Christel, M. Davis, 2017: Seasonal Climate Prediction: A New Source of Information for the Management of Wind Energy Resources. – J. Appl. Meteor. Climatol. **56**, 1231–1247, DOI:10.1175/JAMC-D-16-0204.1.

Worsnop, R.P., J.K. Lundquist, G.H. Bryan, R. Damiani, W. Musial, 2017: Gusts and shear within hurricane eyewalls can exceed offshore wind turbine design standards. – Geophys. Res. Lett. **44**, 6413–6420, DOI:10.1002/2017GL073537.

Zheng, W., H. Wei, Z. Wang, X. Zeng, J. Meng, M. Ek, K. Mitchell, J. Derber, 2012: Improvement of daytime land surface skin temperature over arid regions in the NCEP GFS model and its impact on satellite data assimilation. – J. Geophys. Res. **117**, D06117, DOI:10.1029/2011JD015901.